arXiv:hep-ph/9606201v1 3 Jun 1996

OREXP 96-04

TOP QUARK PHYSICS AT A FUTURE e^+e^- COLLIDER: EXPERIMENTAL ASPECTS[1]

RAYMOND FREY
Physics Department, University of Oregon
Eugene, Oregon 97403, USA
E-mail: rayfrey@bovine.uoregon.edu

ABSTRACT

An overview of top physics and phenomenology at a high-energy linear collider is presented. A comprehensive study of top quark physics is possible at such a facility. The unique threshold production of top pairs would provide measurements of fundamental properties, such as mass and total decay width, to unmatched precision. Above threshold, the full set of Standard Model and anomalous electroweak top couplings can be readily measured with excellent precision. It should also be possible to measure the top Yukawa coupling. This set of measurements would allow a definitive test of the widely held notion that the top quark may play a special role in physics beyond the Standard Model.

1. Introduction

The stage for the future of top physics has been set by the discovery of top at Fermilab this year. While the existence of the top quark has long been expected, its discovery represents a tremendous accomplishment, especially given the incredibly large value of its mass. The published mass values by the CDF and D0 collaborations[1] are $176 \pm 8 \pm 10$ GeV/c^2 and $199^{+19}_{-21} \pm 22$ GeV/c^2, respectively. Thus, we not only have a mass value of $\approx 180 \pm 12$ GeV/c^2 to use for physics studies at future facilities, but such a large value forces one to consider the distinct possibility that the top quark plays a special role in particle physics. At the very least, the properties of the top quark should give important hints of any new physics.

In this context, the determination of a complete set of top properties should be an important goal of the field. A high-energy future linear e^+e^- collider (FLC) provides a very impressive tool to carry out a detailed top-quark physics program. These capabilities have been reported in the previous workshops in this series.[2,3] To a large part, these studies made the top physics case for the FLC. The large mass sets a new tone for the studies, as alluded to above, and in some cases changes the qualitative and quantitative aspects of the measurements. The $t\bar{t}$ threshold becomes

[1] *Presented at Conference on Physics and Experiments with Linear Colliders, Morioka-Appi, Japan, September 1995.*

Supported by Department of Energy contract DE-FG06-85ER40224.

less distinctive, but also less sensitive to accelerator effects. The measurement of top-quark couplings becomes an increasingly important overall goal of FLC physics. The Higgs Yukawa coupling is a fundamental element of the Standard Model, and in non-minimal models of electroweak symmetry breaking, the Yukawa couplings are modified. But since this coupling is proportional to mass, the top quark will likely offer the only possibility for its measurement. There has been much speculation that the large top mass is an indication that, indeed, top has a direct role in the physics of electroweak symmetry breaking, and the large top Yukawa coupling is an indication of this special role.

Nonetheless, there has been some real progress in the FLC top physics analyses since the last workshop. As the accelerator designs have progressed, the parameters which affect the physics have become better determined. The success of the polarized electron beam program at SLC[4] implies that a highly polarized electron beam ($\geq 80\%$) at FLC is easily achievable. This is an important ingredient for the physics, and has been increasingly applied to the FLC studies. The study of couplings directly benefits from polarized beam, and all top physics benefits from the dramatic reduction of the W^+W^- final state with right-handed electron beam. It is also clear that some elements of experimentation at a FLC have yet to be included. In particular, it is clear that secondary vertex detection capabilities should be excellent at the FLC, with important implications for event selection efficiency and purity.

2. Top Production and Decay

The production of top quark pairs in e^+e^- annihilation near threshold is discussed in more detail in the next chapter. Here, we introduce some basic features of Standard Model (SM) open top production, SM top decay, and some broad implications for detection of top decays. There are important radiative effects in high-energy e^+e^- collisions, primarily from initial-state bremsstrahlung and from beamstrahlung, which arises from the large electromagnetic fields produced by the tightly focussed beams at the interaction point. However, due to the energy dependence of the top-pair threshold region, this piece of FLC physics is perhaps most strongly affected by these radiative phenomena. These effects are introduced in Section 2.2, and are discussed in more detail in the context of threshold physics in the next chapter. Most of the basic production and decay information in this section exists in more detail in the proceedings of the previous meetings[2,3] in this series.

The $t\bar{t}$ cross section due to s-channel e^+e^- annihilation mediated by γ, Z bosons increases abruptly at threshold (see Fig. 1), reaches a maximum roughly 50 GeV

above threshold, then falls roughly as the point cross section ($\sigma_{pt} = 87(fb)/s(TeV)$). At $\sqrt{s} = 500$ GeV the lowest-order total cross section for unpolarized beams is 0.54 pb; it is 0.74 (0.34) for a fully left-hand (right-hand) polarized electron beam. With increasing energy t-channel processes resulting, for example, in final states such as $e^+e^-t\bar{t}$ or $\nu\bar{\nu}t\bar{t}$, have increasing cross sections. However, even at 1 TeV these cross sections are still much smaller than those due to the annihilation process, and they are not considered further here. However, in the context of tests of strongly-coupled electroweak symmetry breaking, this $\nu\bar{\nu}t\bar{t}$ process may be of particlular interest, as suggested[5] at this meeting. Theoretical results on single-top production via the process $e^+e^- \to e\nu tb$ were also presented here,[6] and given very high luminosity running at high energy, this offers some attractive physics possibilities, particularly for a V_{tb} measurement. Processes involving Higgs production or exchange, while also having relatively small cross sections, offer the exciting possibility of measuring the Higgs Yukawa coupling. This issue is considered in Chapters 2 and 5.

By far the dominant new influence on top phenomenology is a direct consequence of its large mass: The very large decay width. In the Standard Model the weak decay of top proceeds very rapidly via $t \to bW$ according to

$$\Gamma_t = 0.18(m_t/m_W)^3 \tag{1}$$

For $m_t = 180$ GeV/c^2 this lowest-order prediction is $\Gamma_t = 1.71$ GeV. After first-order QCD and electroweak corrections,[7] this becomes 1.57 GeV. Hence, top decay is much more rapid than the characteristic time for hadron formation, for which the scale is Λ_{QCD}^{-1}.

This implies that the phenomenology of top physics is fundamentally different than that of the lighter quarks. First of all, there will be no top-flavored mesons. While we lose the familiar study of the spectroscopy of these states, we gain unique clarity in the ability to reconstruct the final state. This may prove to be a crucial advantage toward uncovering fundamental issues. The top decay also provides a natural cutoff for gluon emission. In fact, the color strings form along the separating b and $\bar{b}$ quarks. The character of the interference between gluons emitted from top and bottom quarks therefore depends upon the value of Γ_t.[8]

The parton-level decay of top implies that, unlike other quarks, the top spin is transferred to a readily reconstructable final state. Measurement of the $b\bar{b}W^+W^-$ final state therefore provides a powerful means of probing new physics manifested by top with helicity analyses. This is explored in Section 4.2. Another interesting implication of the large m_t is the SM prediction that the decay $t \to bW$ produces mostly longitudinally polarized W bosons, with a degree of longitudinal polarization given by $m_t^2/(m_t^2 + 2M_W^2) \approx 72\%$ for $m_t = 180$ GeV/c^2. This is, in itself, an interesting fact given the important role of longitudinally polarized W bosons in electroweak symmetry breaking.

The luminosity parameters vary somewhat between the various FLC designs. A typical luminosity at $\sqrt{s} = 500$ GeV is 5×10^{33} cm^{-2}s^{-1}, and increases by about a factor two at $\sqrt{s} = 1$ TeV, while the annihilation cross section drops by a factor four. Hence, for a typical assumption of 10^7 seconds of useful running per year, a design year of integrated luminosity at $\sqrt{s} = 500$ GeV is 50 fb^{-1}. This corresponds to roughly 25×10^3 produced $t\bar{t}$ events per design year. An important advantage of e^+e^- colliders is, of course, that the majority of produced events can be used in the physics analyses. Nevertheless, one can anticipate that statistical errors will dominate many measurements. In fact, one of the primary goals of the physics studies is to estimate whether the dominant systematic errors are indeed small.

In the Standard Model $|V_{tb}| \approx 1$, so that the decay mode $t \to bW$ completely saturates the decay width of Eq. 1. Ignoring hard-gluon radiation, the final state is given by the W decay modes from the $b\bar{b}W^+W^-$ intermediate state. Hence, we have the following lowest-order (corrected) decay fractions: BR($t\bar{t} \to b\bar{b}qq'qq'$) = 36/81 (0.455); BR($t\bar{t} \to b\bar{b}qq'\ell\nu$) = 36/81 (0.439); BR($t\bar{t} \to \ell\nu\ell\nu$) = 9/81 (0.106), where $q = u, c$, $q' = d, s$, and $\ell = e, \mu, \tau$. The numbers in parentheses represent these fractions after QCD corrections, which produces a factor of ≈ 1.04 for $W \to qq'$ relative to $W \to \ell\nu$.

Non-standard top decays would, of course, be an interesting addition to top physics. The measurement of the top decay width gives an indirect indication of appreciable new decay modes, and is measurable from the threshold at the level of 10% or better. Studies of a few non-standard decays have been studied. In particular, studies of the modes $t \to bH^+$ and $t \to \tilde{t}\tilde{\chi}$ have been presented[3] and shown to be readily separated with straightforward cuts. It would also be interesting to study the capability for a direct search for non-b top decays. For example, there has been much theoretical interest in t-c-Higgs couplings which could give rise to $e^+e^- \to t\bar{c}$, $\bar{t}c$.

2.1. Event Measurement

Event selection and backgrounds, as discussed in previous reports,[2,3] is briefly summarized here. The $t\bar{t}$ cross section at $\sqrt{s} = 500$ GeV is roughly 0.5 pb. On the other hand, the cross section for lepton and light quark pairs is about 16 pb, while for W^+W^- production it is about 8 pb. The emphasis of most event selection strategies has been to take advantage of the multi-jet topology of the roughly 90% of $t\bar{t}$ events with 4 or 6 jets in the final state. Therefore, cuts on thrust or number of jets drastically reduces the light fermion pair background. In addition, one can use the multi-jet mass constraints M(jet-jet) $\approx M_W$ and M(3-jet) $\approx m_t$ for the cases involving $t \to bqq'$. Simulation studies[9] have shown that multi-jet resolutions of 5

GeV/c^2 and 15 GeV/c^2 for the 2-jet and 3-jet masses, respectively, are adequate and readily achievable with standard resolutions. A detection efficiency of about 70% with a signal to background ratio of 10 was attained in selecting 6-jet final states just above threshold. These numbers are typical also for studies which select the 4-jet+$\ell\nu$ decay mode.

There are two aspects of event selection which should be powerful tools, but have not been widely studied. The background due to W-pair production is the most difficult to eliminate. However, in the limit that the electron beam is fully right-hand polarized, the W^+W^- cross section becomes very small. Hence, even though the beam polarization will be somewhat less than 100%, this allows for experimental control and measurement of the background. On the other hand, the signal is also reduced, to a much smaller degree, by running with right-polarized beam. A possible strategy might be to run with right-hand polarized beam only long enough to make a significant check of the component of background due to W pairs. The left-right W-pair asymmetry predictable at the required few % level.

Another important technique is that of precision vertex detection. The working assumption is that the present experience with SLC/SLD can be used as a model, a rather close model, of what can be done at a FLC. The small and stable interaction point of linear e^+e^- colliders, along with the small beam sizes and bunch-structure timing, make them ideal for pushing the techniques of vertex detection. The present spatial resolution of the CCD vertex detector of SLD is $9 \oplus 29/p(GeV)\sin^{3/2}\theta$ μm in the plane transverse to the beam (θ is the angle with respect to the beamline) and $14 \oplus 29/p(GeV)\sin^{3/2}\theta$ μm in the $r-z$ plane. Equally important is that the primary interaction point is determined equally well. The upshot is that single-hemisphere b-tagging is now done with $\sim$ 40% efficiency and 99% purity, and should improve at a FLC.

Clearly this should have a big impact on FLC top physics, where every event has two high-momentum bottom jets. An event selection strategy should include loose b-tagging criteria. For example, a high efficiency for tagging one b or the other ($\sim$ 90%) could be achieved with reduced purity. This, combined with loose topological and mass cuts to reduce background should provide a very efficient and pure selection. A possible scenario for FLC vertex detection was presented[10] at this meeting. With a large solenoidal magnetic field ($>$ 3 T), the backgound pairs from the beam-beam effects would be confined to a small radius, allowing the inner radius of the CCD detectors to be reduced from 3 cm with SLD to nearly 1 cm. The relatively short bunch trains of the SLAC or JLC designs would make CCDs a good technology choice. The longer TESLA bunch trains may require devices which have a fast-clear capability. In all cases, the beam backgrounds increase rapidly at small radius, hence necessitating the use of some type of pixel technology.

Other detector requirements imposed by top physics are not particularly special.

The one exception is that the measurement of the luminosity function near threshold may require quite good spatial resolution for Bhabha-scattered electrons in the ~ 200 mrad (endcap) region of the detector, presumably involving highly segmented electromagnetic calorimetry. This is discussed further in Section 3. The masks to absorb the beam-induced backgrounds will extend to angles of 100–200 mrad from the beamline. This has a small impact ($\sim 2\%$) on the acceptance for top events. One key point is whether the detector will allow the reconstruction of 6-jet and 8-jet (see Section 5) final states. Generally, jet reconstruction and multi-jet mass resolution is dominated by QCD effects for modern detectors. However, it is important to see if this is still the case for such complicated events.

2.2. Radiative and Beam Effects

All FLC physics analyses must consider the effects of initial-state radiation (ISR) and beamstrahlung (BS) on the spectrum of collision energies. Studies of these effects, as well as the single-beam accelerator energy spread, are presented in the following sections. The effects of ISR are appreciable for high energy electron colliders, where the effective expansion parameter for real photon emission, rather than α/π, is $\beta = \frac{2\alpha}{\pi}(\ln(s/m_e^2) - 1) \approx 1/8$ for $\sqrt{s} = 500$ GeV. Typically, one can use a calculation like that of Kuraev and Fadin[11], which sums the real soft-photon emission to all orders and calculates the initial state virtual corrections to second order. For beamstrahlung, the calculation of Chen[12] provides a good approximation for the effects of beamstrahlung for most FLC designs. The figure of merit for the calculation of beamstrahlung is $\Upsilon = \gamma(B/B_c)$, where $\gamma = E_{beam}/m_e c^2$, B is the effective magnetic field strength of the beam, and $B_c = m_e^2 c^3/e\hbar \approx 4 \times 10^9$ T. When $\Upsilon \ll 1$ the beamstrahlung is in the classical regime and is readily calculated analytically. For example, in the case of the SLAC X-band NLC design, we have $\Upsilon \approx 0.08$ at $\sqrt{s} = 500$ GeV. In this case, there is an appreciable probability for a beam electron (or positron) to emit no photons. So the spectrum is well-approximated as a delta function at $E = E_{beam}$ with a bremsstrahlung-like spectrum extending to lower energies. As we shall see, the delta function piece of the spectrum plays an important role in the shape of the threshold cross section. The NLC design at 500 GeV yields 43% of the luminosity for which the colliding e^+e^- are unaffected by beamstrahlung. It is interesting to note that even in this case there are on average 0.91 emitted photons per beam electron, so multi-photon emission is an important aspect of the calculation.

3. Threshold Physics

The theoretical underpinnings for the process $e^+e^- \to t\bar{t}$ at threshold have been extensively studied,[13] and will not be reproduced here. We will briefly discuss the main features of the expected threshold physics and the measureable parameters. The phenomenolgy associated with the $t\bar{t}$ resonance (toponium) is introduced. A number of studies examining experimental sensitivity to threshold physics have been undertaken. Some of the main implications of these studies are presented.

3.1. Cross Section

In Fig. 1 we show the cross section for $t\bar{t}$ production as a function of nominal center-of-mass energy for $m_t = 180$ GeV/c^2. The theoretical cross section, indicated as curve (a), is based on the results of Peskin and Strassler[14] with $\alpha_s(M_Z^2) = 0.12$, infinite Higgs mass, and nominal Standard Model couplings. Each energy-smearing mechanism, initial-state radiation (b), beamstrahlung (c), and beam energy spread (d), has been successively applied. Hence, curve (d) includes all effects. The beam effects were calculated assuming SLAC X-band NLC design parameters as an example. In this section, the phenomena associated with these curves is discussed, along with the role of accelerator design for the beam effects.

The threshold enhancement given by the predicted cross section curve (a) of Fig. 1 reflects the Coulomb-like attraction of the produced t-$\bar{t}$ due to the short-distance QCD potential

$$V(r) \sim -C_F \frac{\alpha_s(\mu)}{r}\,, \tag{2}$$

where $C_F = 4/3$ and μ is evaluated roughly at the scale of the Bohr radius of this t-$\bar{t}$ toponium atom (labelled θ): $\mu \sim 1/a_\theta = \alpha_s m_t$. This bound state exists, on average, for approximately one classical revolution before one of the top quarks undergoes weak decay. The level spacings of the QCD potential given approximately by the Rydberg energy, $\sim \alpha_s^2 m_t$, turn out to be comparable to the widths of the resonance states, given by $\Gamma_\theta \approx 2\Gamma_t$. Therefore the various toponium states become smeared together, as seen in Fig. 1, where only the bump at the position of the 1S resonance is distinguishable. In fact, for much smaller m_t, or for an anomalously small Γ_t, the various states such as 1S, 2P, 2S, etc. are clearly separated in the theoretical cross section. The infrared cutoff imposed by the large top width also implies[15] that the physics is independent of the long-distance behavior of the QCD potential. The assumed intermediate-distance potential is also found[9] to have a negligible impact. Hence, the threshold physics measurements depend on the short-distance potential

of Eq. 2 based on perturbative QCD. At minimum, a significant qualitative test of QCD is therefore possible, one which goes beyond simply extracting the parameter $\alpha_s(M_Z)$. Perhaps it is possible to perform precise calculations at top threshold, similar to those performed within the context of lattice QCD for the J/ψ or Υ systems, which could be directly confronted with FLC experiment.

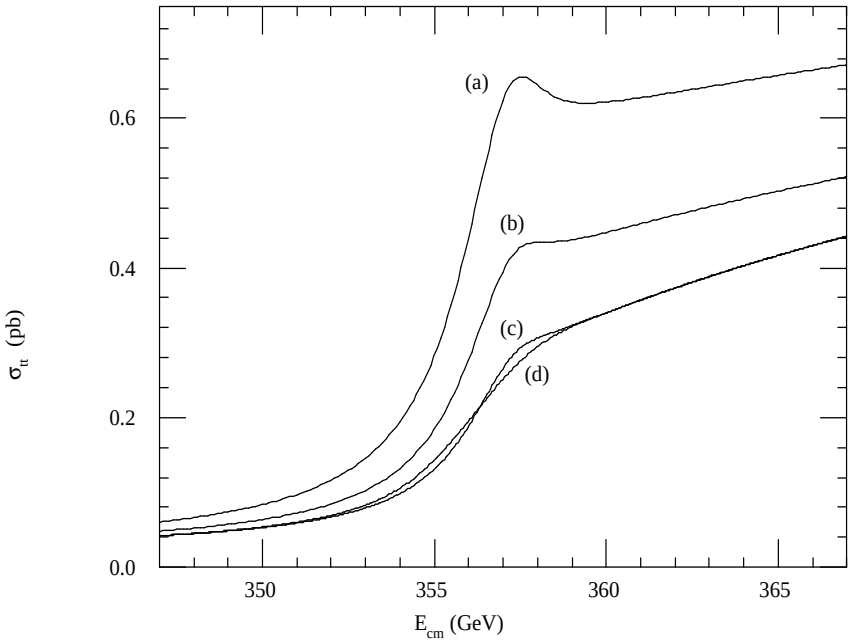


Fig. 1. Production cross section for top-quark pairs near threshold for $m_t = 180$ GeV/c^2. The theoretical cross section is given by curve (a), to which the energy re-distribution effects have been applied. Curve (b): initial-state radiation (ISR); curve (c): ISR and beamstrahlung; curve (d): ISR, beamstrahlung, and beam energy spread.

In increase of α_s deepens the QCD potential, thereby increasing the wave function at the origin and producing an increased 1S resonance bump. In addition, the binding energy of the state increases roughly as the Rydberg energy $\sim \alpha_s^2 m_t$. So the larger α_s has the combined effect of increasing the cross section as well as shifting the curve to lower energy. The latter effect is also what is expected for a shift to lower m_t. Therefore, there exists a significant correlation between the measurments of α_s and m_t from a threshold scan. This is evident from Fig. 10b.

The total top decay width, Γ_t, is an essential piece of exploratory top physics. It is intrinsic to the threshold shape, and is perhaps best measured at threshold. For a quarkonium state, we expect the cross section at the 1S peak to vary with the total

width roughly as $\sigma_{1S} \sim |V_{tb}|/\Gamma_t$, and therefore is very sensitive to the width, as indicated by Fig. 2 for rather wide variations in Γ_t relative to the Standard Model expectation. It is noted that the calculations of Figs. 1 and 2 use the uncorrected top width, as discussed in Section 2.1, so that the resonance structure will actually be more distinctive after correction than that which is shown in these figures. Combining the cross section information with the momentum and asymmetry results, as discussed below, represents what is most likely the best opportunity to measure Γ_t.

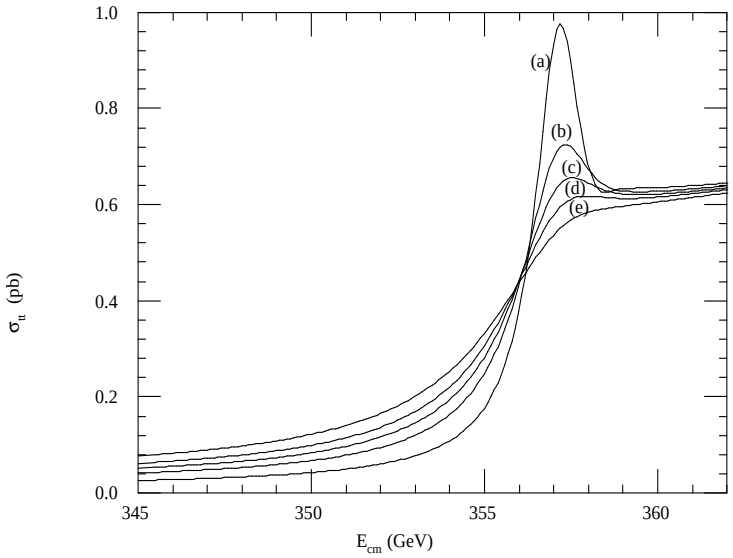


Fig. 2. Variation of theoretical threshold cross section with top width for $m_t = 180$ GeV/c^2. The curves correspond to values of Γ_t/Γ_{SM} of (a) 0.5; (b) 0.8; (c) 1.0; (d) 1.2; (e) 1.5.

In addition to the QCD potential, the t-$\bar{t}$ pair is also subject to the Yukawa potential associated with Higgs exchange:

$$V_Y = -\frac{\lambda^2}{4\pi}\frac{e^{-m_H r}}{r}\,, \tag{3}$$

where m_H is the Higgs mass and λ is the Yukawa coupling, which in the Standard Model is

$$\lambda = \left[\sqrt{2}G_F\right]^{1/2} m_t \tag{4}$$

Because of the extremely short range of the Yukawa potential, its effect is primarily to alter the wave function at the origin, and hence to shift the level of the cross section across the 1S resonance. The Higgs effect at threshold has been carefully

calculated[16] with results shown in Fig. 3. Presumably, the Higgs boson responsible for this enhancement will have already been discovered. So the importance of this measurement would be to check the SM relationship of Eq. 4, which was used in the calculation of Fig. 3.

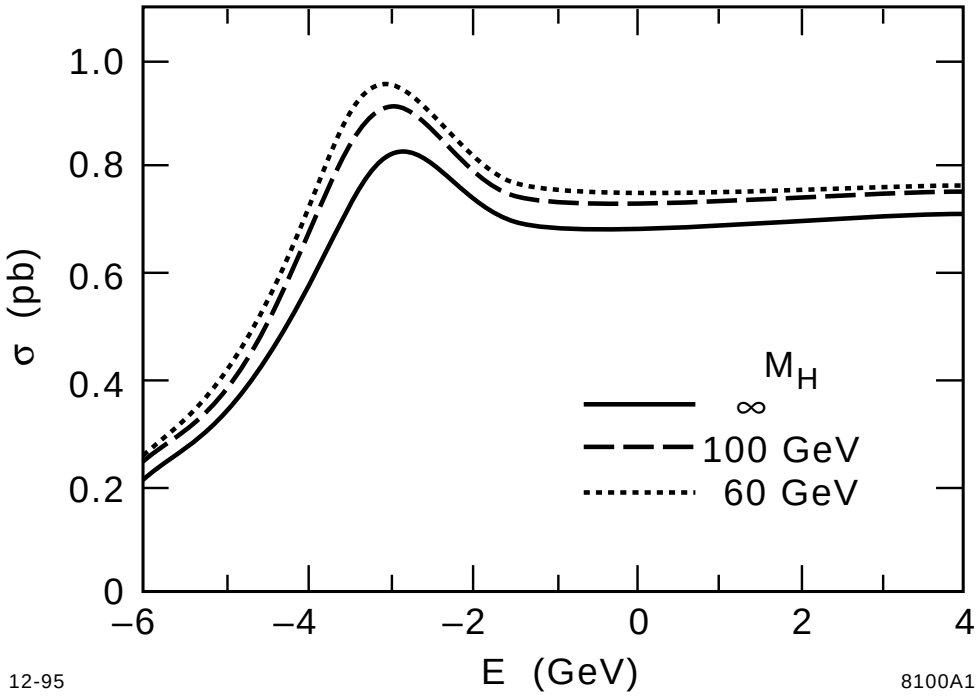


Fig. 3. Theoretical cross section as a function of Higgs mass, from Ref. 16.

This is an exciting possibility, and underscores what could be gained by performing careful threshold measurements. The physics of the threshold cross section is, in summary, expected to depend on the following set of parameters:

$$\sigma = \sigma(m_t, \alpha_s, \Gamma_t, m_H, \lambda) \tag{5}$$

The experimental challenge is to unravel the various dependencies, each of which is qualitatively different, using the cross section scan, as well as the momentum and forward-backward asymmetry measurements discussed in Section 3.3. To do so requires understanding the center-of-mass energy loss mechanisms discussed below.

3.2. Radiative and Beam Effects

The general framework in which calculations of radiative effects was introduced in Section 2.2. Because of the relatively narrow energy structure associated with the top threshold, these effects play a special role. Qualitatively, we can understand these effects in the following way. Both ISR and beamstrahlung (BS) spectra are peaked at zero energy loss, and have long, rather low tails extending to large energy loss. As mentioned previously, the BS spectra is, in fact, quite well modelled by a combination of delta function at zero energy loss plus a synchrotron-like tail. The delta function part, of course, does nothing to disturb the resolution of the threshold. Once the energy loss is greater than $\sim \Gamma_t$, then the corresponding luminosity is lost for threshold physics, but it does not contribute to a smearing in energy of the threshold structure. It is only those portions of the ISR or BS spectra with energy loss $< \Gamma_t$ which contribute to the smearing effects.

Curves (b) and (c) of Fig. 1 indicate the effects of ISR and ISR combined with BS, respectively. Initial-state radiation, of course depends only on the center-of-mass energy. On the other hand, the accelerator designers have some control of the beamstrahlung, which depends on a number of parameters, but can be grossly characterized by the mean field strength $B = 6 \times 10^2$ T. The beamstrahlung calculation of Fig. 1 assumes an NLC X-band design with a parameter set optimized for $\sqrt{s} = 500$ GeV, with spot sizes σ_x and σ_y simply scaled to 360 GeV and with no change in β functions. This is clearly not optimal for luminosity, but should gives a reasonable estimate for the beamstrahlung.

An additional accelerator effect on the threshold shape is that which results from the energy spread of each individual beam in its respective LINAC. The energy spread for a single beam, $\Delta E/E$, can also, to some extent, be controlled by both design and tuning. Generally, a tunable range of ± 50 is possible. Typically, a reduced energy spread results in lower luminosity, while a larger spread produces more backgrounds. As discussed below, the distributions of $\Delta E/E$ at a linear collider, vary according to details of energy compression, RF phasing, and so forth, but are typically not centrally peaked, and so the width is often characterized by a FWHM value. This can have a significant effect on the top threshold shape if the spread is too large. For $m_t = 150$ GeV/c^2, the threshold structure is sharper, meaning that the energy spread effects are more important (see Ref. 9). Curve (d) of Fig. 1 was calculated for a $\Delta E/E$ distribution with FWHM of 0.6%, combined with ISR and BS effects.

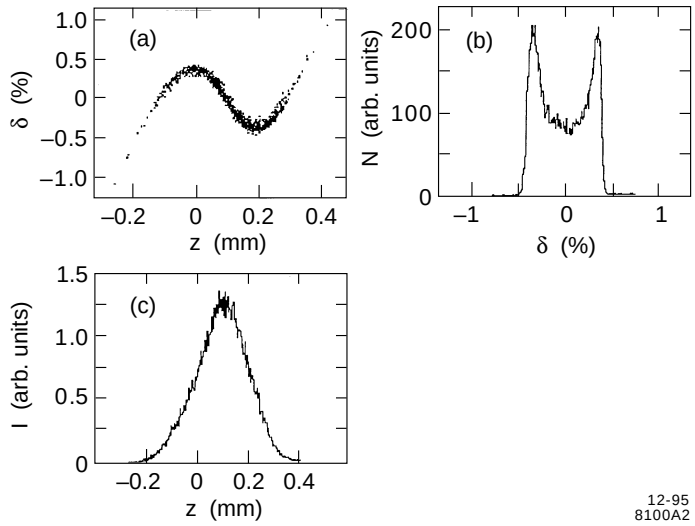


Fig. 4. Expected single-beam energy spread based on SLAC NLC design. (a) Scatter plot of single-beam energy spread, $\delta \equiv \Delta E/E$, versus longitudinal position within a bunch, z, along with projections onto the δ axis (b), and onto the z axis (c).

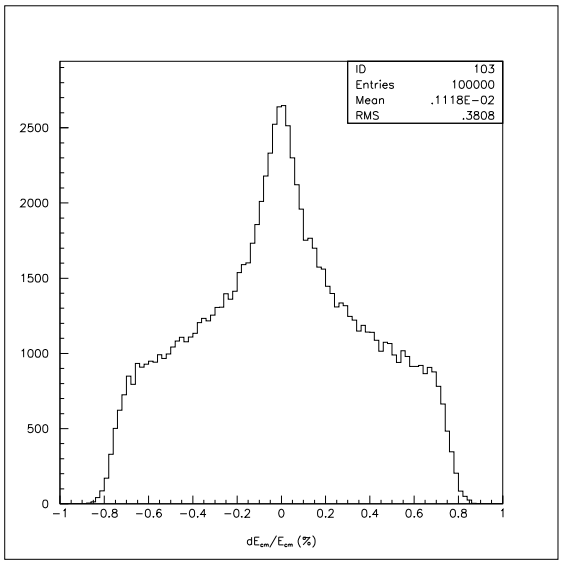


Fig. 5. Distribution of the center-of-mass energy, $\Delta E_{cm}/E_{cm}$, due to the convolution of single-beam energy spread distributions for the two beams. The single-beam energy spread in this case has FWHM of 0.8%, corresponding to the distribution given in Fig. 4.

A few further comments on the beam energy spread are in order. Figure 4 depicts the single-beam energy spread expected[17] for one possible NLC X-band LINAC design. Of course, to determine the effect of these energy spreads on the threshold,

the electron and positron distributions must be convoluted. This, in principle, can be quite complicated. However, a reasonable approach is to ignore transverse chromatic and angular divergence effects, and to simply integrate over collision length. In this way, the luminosity-weighted center-of-mass energy spread, $\Delta E_{cm}/E_{cm}$, is calculated from the single-beam distribution given its dependence on the bunch spatial distribution, as shown in Fig. 4. The resulting distribution for $\Delta E_{cm}/E_{cm}$ is given in Fig. 5. In this case, the input single-beam energy spread has FWHM of 0.8%, corresponding to the distribution shown in Fig. 4. This distribution, in contrast to the single-beam case, is strongly peaked at zero with an RMS of 0.38%, as indicated in the figure. For the NLC, it is expected that the single-beam energy spread can be comfortably adjusted within the FWHM interval 0.6% to 1.0%, and for the top threshold, it is clear that the smaller width is preferred. Curve (d) of Fig. 1 was calculated using the 0.6% width, with a corresponding $\Delta E_{cm}/E_{cm}$ of 0.29%. Figure 6 shows the change in shape of the threshold cross section as the single-beam energy spread is increased. The large top mass of about 180 GeV/c^2 presents a relatively broad, featureless threshold shape which is not nearly as sensitive to the $\Delta E_{cm}/E_{cm}$ distribution as would be expected if the top mass were smaller. Since it is not clear how well this effect could be controlled, this lack of sensitivity is one welcome outcome of the broader threshold.

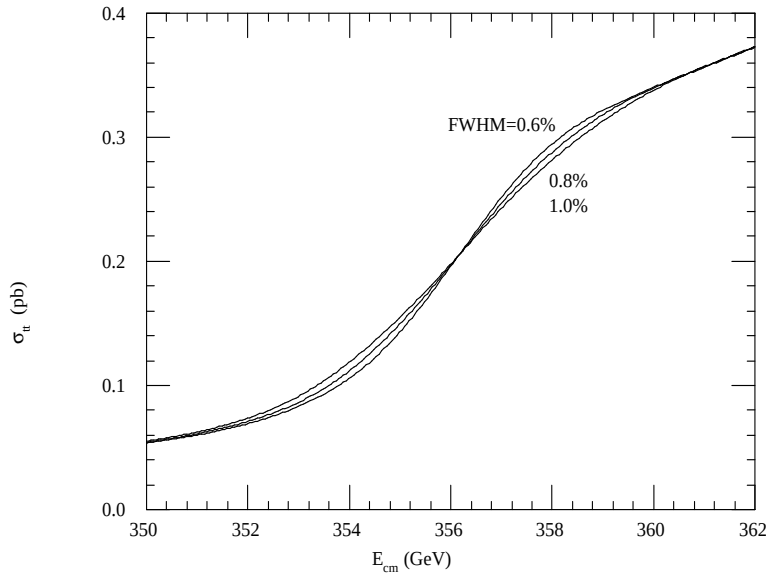


Fig. 6. Comparison of $t\bar{t}$ threshold shape, with all effects included, for different single-beam energy spreads. The three curves correspond to single-beam energy spread distributions with FWHM of 0.6%, 0.8%, and 1.0%, as indicated.

Since the beamstrahlung and LINAC energy spread effects are dependent upon accelerator design, it is interesting to make comparisons at top threshold, where their impact is most apparent. Figure 7 represents a calculation of the top threshold presented[18] at this meeting for a design based on TESLA. We see that the accelerator effects for TESLA are more pronounced than those presented in Fig. 1 for the NLC. This is ascribed to the delta-function component of the beamstrahlung spectrum, discussed earlier, being smaller for the TESLA case. So while the tail of the BS spectrum for TESLA is not as long as that for NLC, which may be advantageous for some physics, the smaller probability for emitting essentially zero BS energy at TESLA results in more energy smearing at top threshold. The bunch length for TESLA is relatively large, thus enabling a passing beam particle many opportunities to emit a small, but non-negligible, amount of radiation.

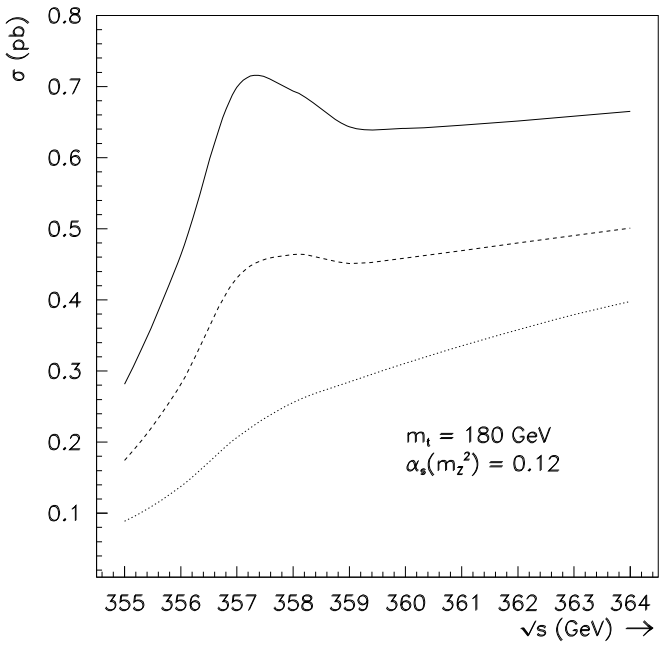


Fig. 7. Top threshold from Ref. 18 assuming $m_t = 180$ GeV/c^2. The accelerator effects are calculated for the TESLA design.

The energy re-distribution effects have an interesting impact on the dependence of the threshold shape on Γ_t. This is shown below in Fig. 8 for which the curves correspond to the theoretical curves of Fig. 2, but with all effects included, in this case assuming NLC parameters. The larger widths give rise to a much flatter shape, but for which the level below the 1S peak is now altered significantly, and provides the best discrimination for the measurement. A physics strategy which is focussed on width optimization would presumably expend a large fraction of the scan luminosity in this region.

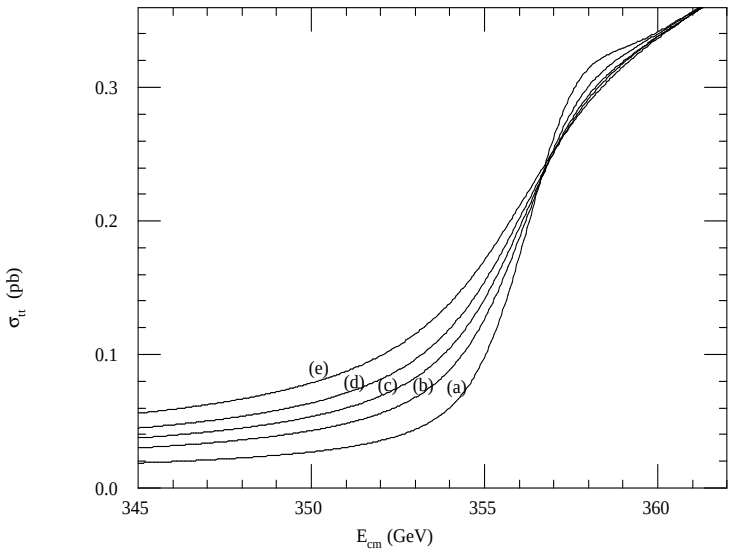


Fig. 8. Variation of threshold cross section with top width, as in Fig. 2, but with initial-state radiation and all beam effects included. A value $m_t = 180$ GeV/c^2 is assumed.

3.3. Momentum and Asymmetry Measurements

As we have discussed, the lifetime of the toponium resonance is determined by the first top quark to undergo weak decay, rather than by annihilation. This has the interesting implication that the kinetic energy (or momentum) of the top daughter particles reflects the potential energy of the QCD interaction before decay. Hence, a measurement of the momentum distribution will be sensitive to V_{QCD} (*i.e.* Eq. 1) and α_s. The theory[19] and phenomenology[9,20] of this physics has been extensively studied. The observable which has been used to characterize the distribution is the momentum, p_p at which the peak of the distribution occurs. The value of p_p at a given center of mass energy is indeed found to be sensitive to α_s.

It is intuitive that a measurement of the threshold cross section is the best method for measuring m_t. However, because of the correlation between m_t and α_s from the cross section, as shown in Fig. 10b, it would be useful to have the momentum measurement be relatively insensitive to m_t. If one defines the scan energy to be with respect to threshold, that is $E = \sqrt{s} - 2m_t$, then this immediately introduces an unwanted dependence on the knowledge of m_t. This is a statement of experimental, as well as theoretical, uncertainty, since the theoretical connection between the threshold shape and m_t is not necessarily exact within an offset of a

few hundred MeV/ c^2. It is better to measure the energy point with respect to a well-defined feature of the experimental threshold curve, as emphasized in Ref. 9, in which it is suggested to measure with respect to the position of the 1S resonance bump, $\Delta E = \sqrt{s} - \sqrt{s_{1S}}$. One expects the average top momentum to vary roughly as the reciprocal of the Bohr radius, or as $\alpha_s m_t$. On the other hand, as we saw earlier, the energy of the 1S resonance is proportional to $-\alpha_s^2 m_t$. So we expect p_p as a function of ΔE to be approximately independent of m_t, but to retain sensitivity to α_s. In fact, this is borne out in Figs. 9a and 9c. As the top width increases, the top decays occur at shorter distances, therefore shifting the momenta to larger values. This can be seen in Fig. 9b. Therefore the momentum spectra can be used, in conjunction with the cross section points, to separate the measurements of m_t, α_s, and $|V_{tb}|$, or Γ_t. For $\Delta E \approx 2$ GeV or greater, the use of p_p was found[9,18] to be very insensitive to ISR and beam effects for both JLC and TESLA designs.

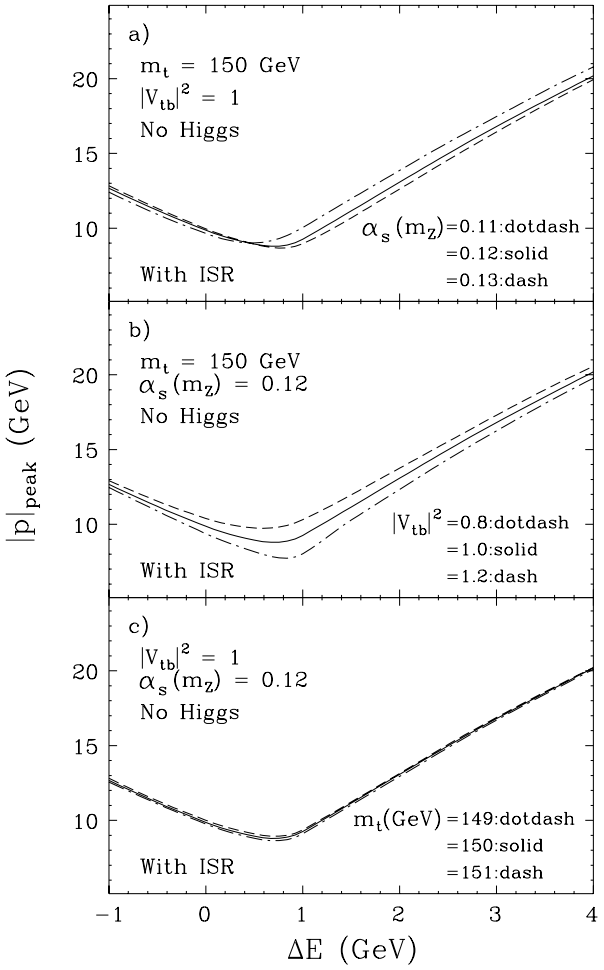


Fig. 9. Position of top peak momentum as a function of scan energy for different values of the following physics input parameters (from Ref. 9). (a) α_s; (b) $|V_{tb}|$; (c) m_t.

A quite different observable has been studied[21,9] to help further pin down the physics parameters at threshold. Top is produced symmetrically when produced in the 1S state. The vector coupling present with Z-t-$\bar{t}$ and γ-t-$\bar{t}$ can proceed to S and D-wave resonance states. On the other hand, the axial-vector coupling present with Z-t-$\bar{t}$ gives rise to P-wave resonance states. Hence, it is possible to produce interference between S and P-waves which gives rise to a forward-backward asymmetry (A_{FB}) proportional to $\beta\cos\theta$. Because of the large width of the resonance states, due to the large Γ_t, these states do overlap to a significant extent, and a sizeable A_{FB} develops. The value of A_{FB} varies from about 5% to 12% across the threshold, with the minimum value at about $\sqrt{s_{1S}}$. Since the top width controls the amount of S-P overlap, we expect the forward-backward asymmetry to be a sensitive method for measuring Γ_t.

3.4. Measurement of the Physics Parameters

A number of studies have been carried out to simulate measurements at $t-\bar{t}$ threshold. Figure 10a depicts a threshold scan[9] for which an integrated luminosity of 1 fb^{-1} has been expended at each of 10 values of nominal center-of-mass energy, $\sqrt{s}$. A value of $m_t = 150$ GeV/c^2 was used. In this case the 6-jet final state was selected, giving a branching fraction times detection efficiency of 30%. The physics background is measured by the scan data taken below threshold. No beam polarization is assumed. A fit of the data points to the theoretical cross section, including all radiative and beam effects discussed above, results in a sensitivity for the measurement of m_t and α_s shown in Fig. 10b. The correlation between these two parameters, as discussed in Section 3.1, is apparent. Even for the modest luminosity assumed here, the cross section measurement gives quite good sensitivity to these quantities. If no prior knowledge is assumed, errors for m_t and α_s are 200 MeV/c^2 and 0.005, respectively. Clearly, the value of $\alpha_s(M_Z^2)$ is already known at LEP/SLC to this same level of precision, implying that m_t is considerably better determined, approaching 100 MeV/c^2 in the limit where $\alpha_s(M_Z^2)$ is known exactly. This same cross section scan of 11 fb^{-1} also implies sensitivity to Γ_t and the Yukawa coupling, λ, of 0.2 and 0.3, respectively. As described earlier, the measurement of the top momentum and its forward-backward asymmetry can contribute valuable additional information. The top momentum measusurement alone produces a sensitivity corresponding to errors for α_s and $|V_{tb}|$ of 0.002 and 0.04, respectively, assuming an integrated luminosity of 100 fb^{-1}. The the position of the 1S peak is assumed to be well known from the cross section scan. The optimal energy for the momentum measurement is $\Delta E = \sqrt{s} - \sqrt{s_{1S}} \approx 2$ GeV. The A_{FB} measurement at $\Delta E \approx 1$ GeV provides an important crosscheck of the total width and of α_s, but

requires more than twice the luminosity relative to the momentum measurement to provide similar sensitivity. We see that while the cross section scan gives most of the sensitivity to the threshold parameters, the momentum measurement in particular significantly increases sensitivity to the top width measurement. Similar threshold studies have been presented[2,3] at previous meetings, with similar results.

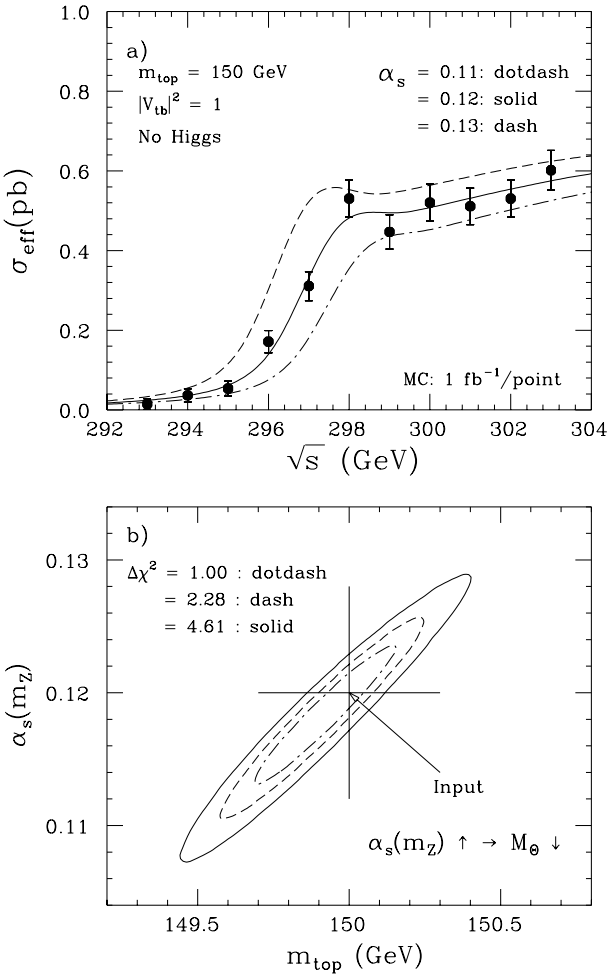


Fig. 10. (a) Top threshold scan from Ref. 9; (b) corresponding error ellipse for m_t and α_s. A value for m_t of 150 GeV/c^2 was assumed.

At this meeting, new threshold studies by the European Working Group[18] were presented assuming $m_t = 180$ GeV/c^2 and TESLA beam parameters. The cross section scan consisted of 10 points, each of 5 fb^{-1} per point, with one of the points below threshold to measure background. With an event selection consisting of topological and mass cuts, the efficiency for 6-jet events was 33% with a signal to background ration of 5.5. A 2-parameter fit to m_t and α_s yielded errors of 250 MeV/c^2 and 0.006, assuming no previous knowledge of these parameters. The single-parameter sensitivities are 120 MeV/c^2 and 0.0025 for m_t and α_s, respectively. When the top

momentum information for 4-jet+$\ell + \nu$ events from this same scan was included in the fit, the 2-parameter fit errors improved to 200 MeV/c^2 and 0.005 for m_t and α_s, respectively. This analysis differs in principle from the one that of Ref. 9 in that the scan energy used is $\sqrt{s} - 2m_t$ rather than $\sqrt{s} - \sqrt{s_{1S}}$, as discussed in Section 3.3. This has the efffect that the momentum measurement also produces a strong correlation between m_t and α_s. However, since this correlation is different from the one resulting from the cross section scan, the two can still be disentangled. The 4-jet+$\ell + \nu$ events were also studied in an analysis of the forward-backward asymmetry. These events were reconstructed with a 15% efficiency and a charge mis-identification rate of 3%. With the same 50 fb^{-1}, the A_{FB} measurement, in conjunction with the cross section and momentum measurements, gave a slight improvement in the Γ_t sensitivity of 18%. However, it is clear, following Ref. 9and from Fig. 9, that threshold measurements optimized for the Γ_t measurement should be able to achieve a sensitivity of 5–10% for 50 fb^{-1} and $m_t = 180$ GeV/c^2. The m_t-α_s error ellipse resulting from these measurements is shown in Fig. 11.

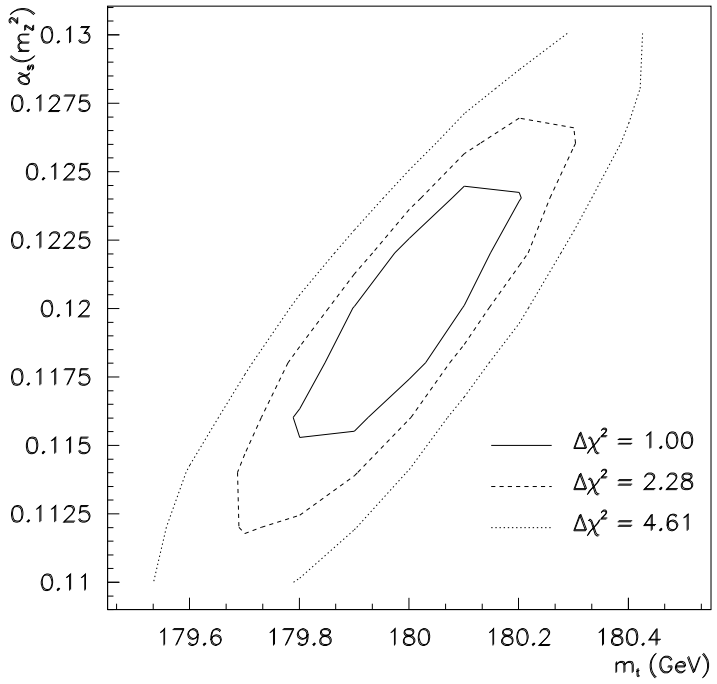


Fig. 11. Error ellipse for m_t and α_s using cross section, momentum peak, and forward-backward asymmetry information from Ref. 18. Mass and integrated luminosity values of $m_t = 180$ GeV/c^2 and 50 fb^{-1}, respectively, are assumed.

3.5. Measurement of Luminosity Spectrum

A unique experimental aspect of top threshold physics is the necessity for knowledge of the integrated luminosity as a function of the effective center of mass, or collision, energy. A design year of data, after event selection, would result in an event sample of $\sim 10^4$ events, and hence an overall statistical error of roughly 1%. Therefore, we would hope to measure the luminosity expended at each scan point at a level approaching this 1%. This requires knowledge of the luminosity spectrum, $d\mathcal{L}/dE_{cm}$, at a level commensurate with these errors. The nominal center-of-mass energy, $\sqrt{s}$, can in principle be measured using the same methodology as that presently used at the SLC,[22] in which a precision magnetic spectrometer is applied to the individual beams after passing through the interaction point. An absolute energy measurement of ~ 20 MeV is achieved. At a FLC, this same method would be applied, where one beam at a time would be turned off in order to eliminate ISR and BS losses. One would want to measure $\sqrt{s}$ with an error of ~ 100 MeV, which results from simply scaling the SLC spectrometer from M_Z to $2m_t$.

One might imagine that $\sqrt{s}$ including the energy loss due to beamstrahlung could be measured with this same spectrometer and with the beams put into collision. However, this is not really the correct measurement, since for the physics collisions the energy is luminosity sampled, whereas the average beamstrahlung loss results from what is, in principle, different sampling. One would hope instead to measure a physics quantity which is subject to exactly the same luminosity spectrum as that of $t-\bar{t}$ production. This has been studied in Ref. 23, where a program for carrying out a measurement of $d\mathcal{L}/dE_{cm}$ was proposed. The basic idea is to measure a $2 \to 2$ process, such as Bhabha scattering, where the final-state acollinearity, θ_A, can be measured in the detector to good accuracy. The acollinearity is related to the difference in the two beam energies, δE, according to $\theta_A = (\delta E/E)\sin\theta$ for small θ_A, where θ is the scattering angle. The distribution in θ_A must then be related to $d\mathcal{L}/dE_{cm}$. The effects of ISR, beamstrahlung, and single-beam energy spread on both θ_A and luminosity spectra can be calculated. This connection was modelled in Ref. 23, where it was found that a measurement error for θ_A at the level of 0.1% is sufficient. Bhabha scattering has a high rate, of order 10^2 times that for top production, depending upon the angular region used, and hence would be a good candidate for this measurement. Angular resolutions at the requisite level should be possible using high-granularity electromagnetic calorimetry, for example using silicon strip readout layers.

It is important to confirm using real distributions and beam parameters that this scheme can be carried out, and that the requisite measurement errors are

possible. The beam parameters will change with time at some level, and hence the contribution to the luminosity spectrum of beamstrahlung, which strongly depends on these parameters, will also change with time. Of course, in the scheme outlined above, these variations will simply be incorportated into the measured luminosity spectra by means of the high-rate Bhabha scattering. However, the connection between luminosity and acollinearity spectra using this technique should be carefully checked using realistic calculations.

4. Top Couplings

The motivation to examine non-standard top couplings is clear, particularly in view of the large top mass. There are a number of models of electroweak symmetry breaking for which a heavy top quark is either an important or essential element. In any case, as by far the heaviest known particle, it is important to examine all top properties in as general and complete a manner as possible. In this section, we investigate the sensitivity of a high-energy e^+e^- linear collider toward carrying out a general program of top quark coupling measurements. As we shall see, helicity amplitudes are an important element of these studies, and the methods here make use of the expected highly-polarized electron beam.

These studies make some basic assumptions of top properties. As discussed before, with a mass of 180 GeV/c^2 it is expected that top will decay before it hadronizes. Thus, in its decay, $t \to bW$, the top spin information is directly transferred to the final state. This offers the unique opportunity to perform a conceptually clean helicity analysis by means of top event reconstruction, in particular with the relatively clean final states available at a FLC, and in this way sensitively probe the top couplings. In the following sections, we briefly review the formalism for angular distributions expected in top production and decay, and how these are affected by non-standard couplings. We confine our discussion here to the study of anomalous electroweak top couplings. A discussion of anomalous QCD coupling (chromomagnetic moments) has been presented[24] separately at this meeting.

4.1. Angular Distributions and Couplings

The top neutral-current coupling can be generalized to the following form for the Z-t-$\bar{t}$ or γ-t-$\bar{t}$ vertex factor:

$$\mathcal{M}^{\mu(\gamma,Z)} = e\gamma^\mu \left[Q_V^{\gamma,Z} F_{1V}^{\gamma,Z} + Q_A^{\gamma,Z} F_{1A}^{\gamma,Z} \gamma^5 \right] + \frac{ie}{2m_t} \sigma^{\mu\nu} k_\nu \left[Q_V^{\gamma,Z} F_{2V}^{\gamma,Z} + Q_A^{\gamma,Z} F_{2A}^{\gamma,Z} \gamma^5 \right], \quad (6)$$

which reduces to the familiar SM tree level expression when the form factors are $F_{1V}^{\gamma} = F_{1V}^{Z} = F_{1A}^{Z} = 1$, with all others zero. The quantities $Q_{A,V}^{\gamma,Z}$ are the usual SM coupling constants: $Q_V^{\gamma} = Q_A^{\gamma} = \frac{2}{3}$, $Q_V^{Z} = (1 - \frac{8}{3}\sin^2\theta_W)/(4\sin\theta_W\cos\theta_W)$, and $Q_A^{Z} = -1/(4\sin\theta_W\cos\theta_W)$. The non-standard couplings $F_{2V}^{\gamma,Z}$ and $F_{2A}^{\gamma,Z}$ correspond to electroweak magnetic and electric dipole moments, respectively. While these couplings are zero at tree level in the SM, the magnetic dipole coupling is expected to attain a value $\sim \alpha_s/\pi$ due to corrections beyond leading order. On the other hand, the electric dipole analog term violates CP and is expected to be zero in the SM through two loops.[25] Therefore, the search for a non-zero value is very interesting. Such a non-standard coupling necessarily involves a top spin flip, hence the coupling is proportional to m_t.[26]

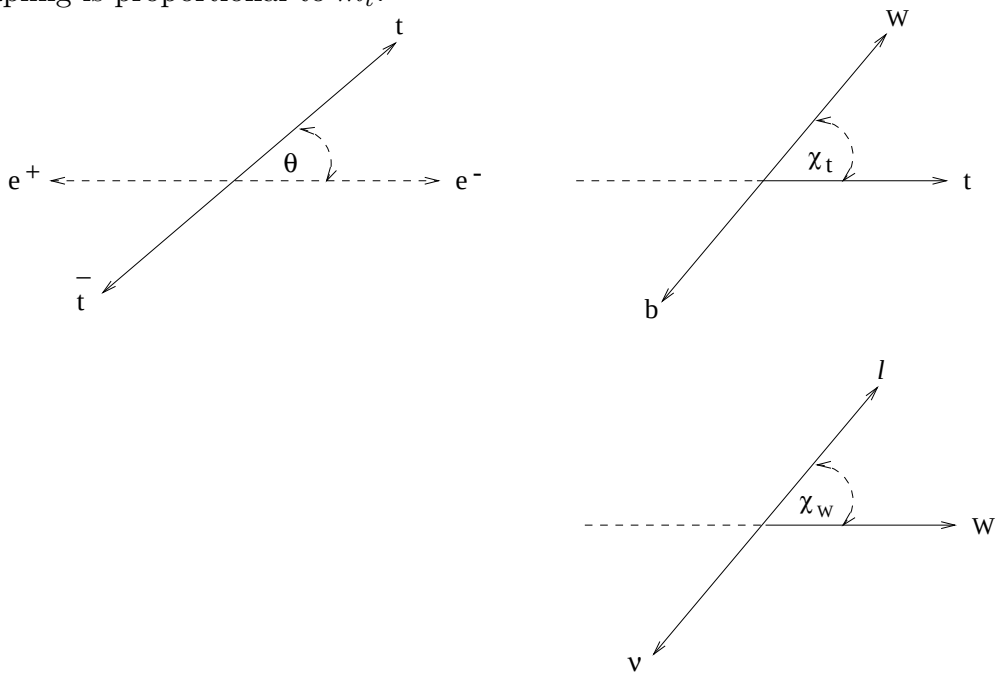


Fig. 12. Definitions of helicity angles. (a) Production angle θ in $t\bar{t}$ proper frame; (b) χ_t measured in the top proper frame as shown; and (c) χ_W in the W proper frame.

In terms of helicity amplitudes, the form factors obey distinct dependences on the helicity state of e^-, e^+, t, and $\bar{t}$, which can be accessed experimentally by beam polarization and the measurement of the decay angles in the final state. These helicity angles can be defined as shown in Fig. 12. The angle χ_W is defined in the W proper frame, so that the W arrow represents its momentum vector in the limit of zero magnitude. The analgous statement holds for the definition of χ_t. Experimentally, all such angles, including the angles corresponding to χ_t and χ_W for the $\bar{t}$ hemisphere, are accessible. This requires full event reconstruction. Given the large number of constraints available in these events, full reconstruction is entirely feasible, and is discussed further in Section 4.2. However, to reconstruct θ one

must also take into account photon and gluon radiation in the event reconstruction. As discussed earlier, photon radiation from the initial state is an important effect. But this is to excellent approximation a purely longitudinal boost which can be handled by demanding longitudinal momentum balance. Gluon radiation can be more subtle. Jets remaining after reconstruction of t and $\bar{t}$ can be due to gluon radiation from t or b, and the correct assignment must be decided based on the kinematic constraints and the expectations of QCD.

Table 1. Dependence of the helicity amplitudes on top production angle (see Fig. 12) and on the various neutral-current form factors. The helicity components for e^-, e^+, t, and $\bar{t}$ define the helicity amplitude and are given in the first column, where L= $-$ and R= $+$; the angular dependence is given by $f(\theta)$; and the applicable form factors are given in the last column.

$h(e^-), h(e^+), h(t), h(\bar{t})$	$f(\theta)$	form factors
$\pm$,$\mp$,$-$,$-$	$\sin\theta$	F_{1V}, F_{2V}, F_{2A}
$\pm$,$\mp$,$-$,$+$	$1+\cos\theta$	F_{1V}, F_{1A}
$\pm$,$\mp$,$+$,$-$	$1-\cos\theta$	F_{1V}, F_{1A}
$\pm$,$\mp$,$+$,$+$	$\sin\theta$	F_{1V}, F_{2V}, F_{2A}

The dependencies of the neutral current couplings to measurement of the distribution of the production angle θ are outlined in Table 1. The initial state helicity is defined by the beam polarization, and the final state is determined by measurement of the angular distributions. The explicit formulae for the form factors can be found in Ref. 28. In the case of the production angle θ, the SM expectations[27] are given in Fig. 13 for the various $t\bar{t}$ helicity combinations and for left and right-hand polarized electron beam. We see, for example, that for left-hand polarized electron beam, top quarks produced at forward angles are predominantly left handed, while forward-produced top quarks are predominantly right handed when the electron beam is right-hand polarized. These helicity amplitudes combine to produce the following general form for the angular distribution:[28]

$$\frac{d\sigma}{d\cos\theta} = \frac{\beta_t}{32\pi s}\left[c_0\sin^2\theta + c_+(1+\cos\theta)^2 + c_-(1-\cos\theta)^2\right], \qquad (7)$$

where c_0 and $c_\pm$ are functions of the form factors. The helicity structure of the event is highly constrained by beam polarization and production angle. Clearly, the measurement of production angle from event reconstruction, as well as the beam polarization, powerfully constrain any non-standard contibutions to the form factors.

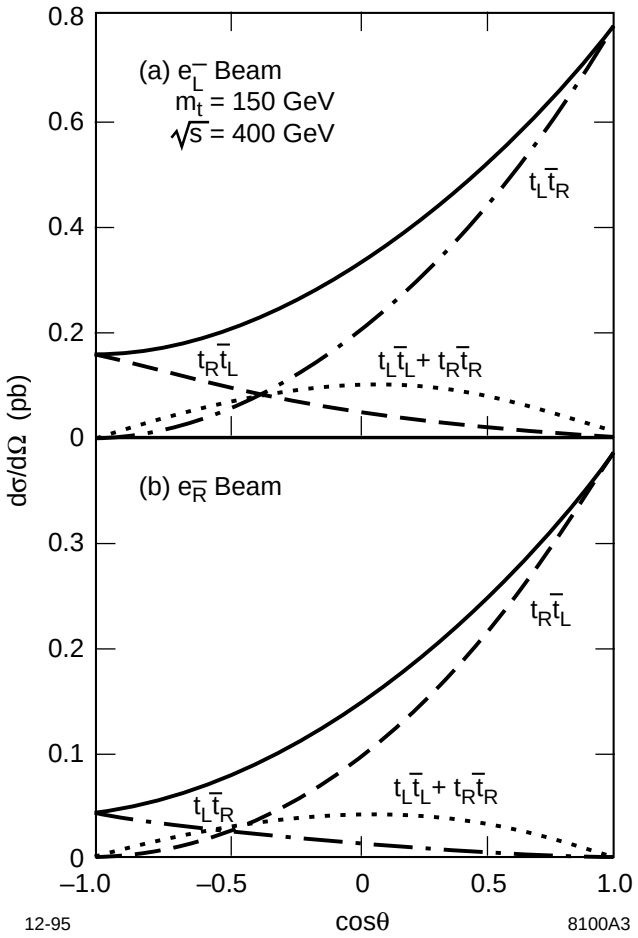


Fig. 13. Production angle for $t\bar{t}$ for the possible final-state helicity combinations, as indicated, for (a) left-polarized electrons, and (b) right-polarized electrons. The complete cross sections are the solid curves.

For the top charged-current coupling we can write the W-t-b vertex factor as

$$\mathcal{M}^{\mu,W} = \frac{g}{\sqrt{2}}\gamma^\mu \left[P_L F_{1L}^W + P_R F_{1R}^W\right] + \frac{ig}{2\sqrt{2}\,m_t}\sigma^{\mu\nu}k_\nu \left[P_L F_{2L}^W + P_R F_{2R}^W\right], \quad (8)$$

where the quantities $P_{L,R}$ are the left-right projectors. In the SM we have $F_{1L}^W = 1$ and all others zero. The form factor F_{1R}^W represents a right-handed, or $V + A$, charged current component. The form of the angular distribution expected for each helicity combination at the W-t-b vertex factor is given in Table 2, as well as the relevant form factor. Similarly, the angular dependence for the W decay is given in Table 3, where the SM couplings are assumed in this case. Note that, as mentioned earlier, the case where the W is longitudinally polarized is particularly relevant for heavy top.

Table 2. Dependence of the helicity amplitudes on the helicity angles, as defined in Fig. 12, and on the charged-current form factors. The helicity states for t and b are indicated by $\pm$, as in Table 1. The longitudinal polarization state of W is indicated by 0.

$h(t), h(b), h(W)$	$f(\chi_t)$	form factors
$-,-,-$	$\cos\chi_t/2$	F_{1L}, F_{2R}
$-,-,0$	$\sin\chi_t/2$	F_{1L}, F_{2R}
$+,-,-$	$\sin\chi_t/2$	F_{1L}, F_{2R}
$+,-,0$	$\cos\chi_t/2$	F_{1L}, F_{2R}
$-,+,+$	$\sin\chi_t/2$	F_{1R}, F_{2L}
$+,+,+$	$\cos\chi_t/2$	F_{1R}, F_{2L}
$-,+,0$	$\cos\chi_t/2$	F_{1R}, F_{2L}
$+,+,0$	$\sin\chi_t/2$	F_{1R}, F_{2L}

Table 3. Helicity angle dependence for W decay, as defined in Fig. 12. The longitudinal polarization state of W is indicated by 0.

$h(W)$	$f(\chi_W$
$-$	$\sin^2\chi_W/2$
$+$	$\cos^2\chi_W/2$
0	$\sin\chi_W$

4.2 Form Factor Analyses

Three analyses of form factor measurement were presented in the parallel session. These analyses are typical of those in the literature. Cuypers[26] designed an analysis which is specifically sensitive to the electroweak dipole moments, $F_{2A}^{\gamma,Z}$. Two CP odd observables are used: $(\vec{p_b}\times\vec{p_{\bar{b}}})\cdot\hat{z}$ and $(\vec{p_b}+\vec{p_{\bar{b}}})\cdot\hat{z}$, where $\hat{z}$ is along the incoming e^+. The first observable is CPT even and probes the real part of the dipole moment, whereas the second is CPT odd and probes the imaginary part. The results show, for example, that for an integrated luminosity of 20 fb^{-1} at $\sqrt{s}=750$ GeV, then the 95% CL limits on the real part of the dipole moment, $\Re(F_{2A}^Z)$, correspond to a dipole moment of about 10^{-19} e-m. Efficiencies for b and W tagging of 10% were assumed. Electron beam polarization is an important element of this analysis, and allows an increased sensitivity relative to similar analyses performed without the

assumption of beam polarization.

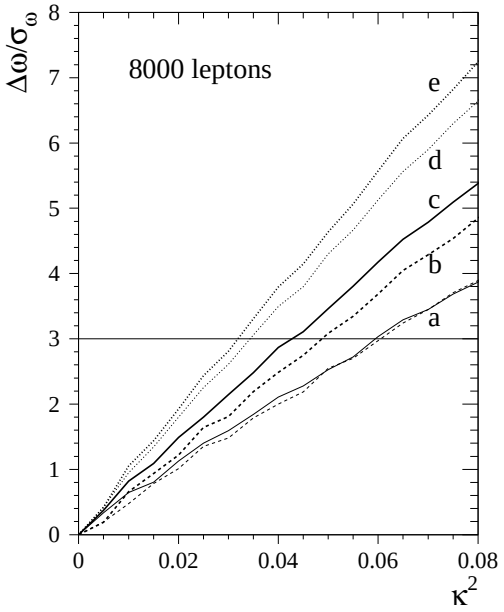


Fig. 14. Sensitivity to the measurement of an anomalous top charged-current coupling from Ref. 18. The curves a through e represent including incrementally more information in the event reconstruction.

Martinez presented[18] two form factor analyses, where the emphasis was on examining the effects of including full Monte Carlo event generation and realistic detector resolutions. In the first analysis, the neutral-current couplings were examined by searching for a non-zero term proportional to $\sin^2\theta$ (see Eq. (5) and Table 1). For $\sqrt{s}$ = 500, 50 fb^{-1}, and no beam polarization, it was found that such a non-standard coupling could be constrained to zero with a 68% CL limit of 1.5% (relative to SM coupling) for an ideal detector, increasing to $\approx$ 4% after detection efficiency, detector resolution, t–$\bar{t}$ mis-asignment, and backgrounds were included. An analysis of the charged-current coupling was performed at $t-\bar{t}$ threshold assuming 100 fb^{-1} of data with no polarization. Threshold was chosen so that the lab and center of momentum frame lepton momenta from top decay are not very different. In this case, since the top spin is oriented along the beam line, the helicity angle χ_t is effectively measured directly in the laboratory frame once the $W \to \ell\nu$ is reconstructed. In Fig. 14 the sensitivity for measuring the quantity κ is displayed, where the SM couplings are modified according to $g_v = (1+\kappa)/\sqrt{1+\kappa^2}$ and $g_a = (-1+\kappa)/\sqrt{1+\kappa^2}$. The sensitivity is expressed in terms of the deviation from the SM by a single quantity ω divided by its measurement error, σ_ω. As

more information is included, the sensitivity increases, as indicated by the curves *a*–*e*. It would be interesting to compare the sensitivity using this technique at threshold with one well above threshold which relies upon event reconstruction and constraints.

4.2.1 Full-Event Analysis

We now discuss in more detail an analysis which can be applied in a general way to the study of top couplings. The results presented are limited in extent and are of a preliminary nature, but the methodology readily allows including more experimental detail. We use $m_t = 180$ GeV/c^2. The only center-of-mass energy considered here is 500 GeV. It should be repeated at higher energy. We consider an integrated luminosity of 10 fb^{-1}, which is quite reasonable given a typical design luminosity of 5×10^{33} cm^{-2}s^{-1}. The decays are assumed to be $t \to bW$ followed by $WW \to \ell\nu\, qq'$. Now, since the top production and decay information is correlated, it is possible to combine all relevant observables to ensure maximum sensitivity to the couplings. In this study, a likelihood function is used to combine the observables. The key tool for this study is the Monte Carlo generator developed by Schmidt,[29] which includes $t\bar{t}(g)$ production to $\mathcal{O}(\alpha_s)$. No hadronization is performed. Most significantly, the Monte Carlo correctly includes the helicity information at all stages.

In general, one needs to distinguish t from $\bar{t}$. The most straightforward method for this is to demand that at least one of the W decays be leptonic, and to use the charge of the lepton as the tag. One might imagine using other techniques, for example with topological secondary vertex detection one could try to distinguish b from $\bar{b}$. Also, if the neutral-current couplings are determined and the charged-current coupling is being studied in more detail, one could then use the polarization and production angle to tag t versus $\bar{t}$, as indicated by Fig. 13. However, here it is simply assumed that one W decays hadronically and the other W decays to electron or muon:

$$t\bar{t} \to b\bar{b}WW \to b\bar{b}q\bar{q}'\ell\nu, \tag{9}$$

where $\ell = e, \mu$. The branching fraction for this decay chain is 24/81. The top decay products, including any jets due to hard gluon radiation, must be correctly assigned with good probability in order to carry out this analysis. The correct assignments are rather easily arbitrated using the W and top mass constraints. The effects of initial-state radiation and beamstrahlung give rise to events in which the $t\bar{t}$ longitudinal momentum is unbalanced. This implies that additional information must be included in order to determine the longitudinal momentum, p_z^ν, of the neutrino in $W \to \ell\nu$. In fact, Ladinsky and Yuan have shown[28] that the m_W and m_t constraints determine p_z^ν, with the correct sign, with an efficiency of about

70%. They also show, indeed, that events with doubly-leptonic W decays can also be correctly reconstructed with good efficiency. For simplicity, we ignore this additional event fraction (BR= 4/81 assuming $\ell = e, \mu$).

The Schmidt Monte Carlo is used to generate $t\bar{t}(g)$ with full $\mathcal{O}(\alpha_s)$ corrections. Simple, phenomenological detection resolution functions are then applied to the decay chain of Eq. (4). It is assumed that the leptons and quarks are measured with an energy resolutions of $\Delta E/E = 0.15/\sqrt{E(GeV)}$ and $\Delta E/E = 0.40/\sqrt{E(GeV)}$, respectively. The direction of quark momenta is assumed to be precisely determined. The missing energy is then assumed to have a resolution which is the quadrature sum of the lepton and quark measurement errors. It is important to check the sensitivity of these obvious over-simplifications to the results by applying experimental resolution functions to fully hadronized events. Nonetheless, it is likely that the most important effect of full event simulation may instead be due to jet mis-identification in these rather complicated 4(or 5)-jet final states. In fact, we determine the RMS spread of the reconstructed top mass distribution to be ≈ 8 GeV, which is not very different from the results based on simulations[3] which include jet fragmentation. It will also be interesting to apply what is expected to be highly efficient b-jet tagging in order to reduce jet combinatorial inefficiency. The acceptance is conservatively assumed to be zero for angles within 10° of the beamline (forward and backward) due to the dead-cone masking. This represents an inefficiency of only 3%. Electron beam polarization is assumed to be $\pm 80\%$.

Once the events are fully reconstructed, the resulting helicity angles (see Fig. 12) are then used to form a likelihood which is the square of the theoretical amplitude for these angles given an assumed set of form factors. The likelihood is usually examined while a single form factor value is varied from its nominal SM value. A typical result is given in Fig. 15, in this case for a hypothetical right-hand W-t-b coupling. The overall efficiency of the analysis, including branching fractions, reconstruction efficiency, and acceptance, is about 18%. This implies an event sample of about 1400 events for 10 fb^{-1} of luminosity with $\sqrt{s} = 500$ GeV and $m_t = 180$ GeV/c^2.

In the case shown in Fig. 15, the use of beam polarization produces an obvious increase in sensitivity, as evidenced by the steeper likelihood curve. In many cases, because the helicity structure of these events is highly constrained by the Standard Model, the polarization information is often seen to be formally redundant. However, several points should be made. First, an additional powerful experimental tool is generally found to be required, rather than redundant, once all of the real-world uncertainties are included. In addition, it may be the case that more than a single coupling is found to exhibit an apparent deviation from its nominal SM value. Polarization will likely allow the effects to be separated. A left-hand polarized electron beam will always give a statistical advantage in the SM for $t\bar{t}$ production. The

cross sections are 680 fb, 360 fb, and 520 fb for 80% left-polarized beam, unpolarized beam, and 80% right-polarized beam, respectively. In addition, as mentioned previously, the fact that the W^+W^- background goes away completely in the limit of a fully right-polarized beam implies that its level is subject to direct verification in the data.

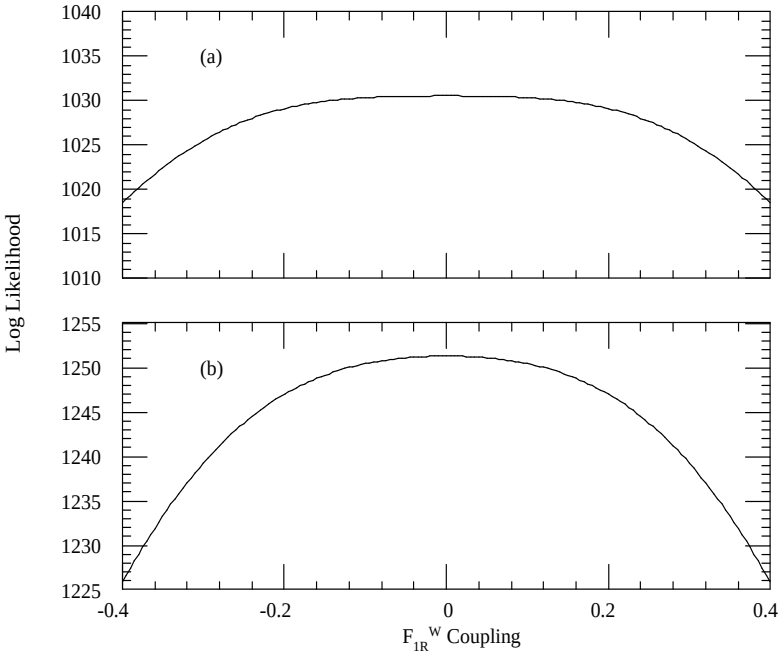


Fig. 15. An example of the variation of the logarithm of the likelihood funtion as a function of coupling strength. In this case the coupling is a hypothetical right-handed top charged-current coupling, F_{1R}^W, for (a) unpolarized beams, and (b) an 80% left-polarized electron beam.

Table 4 shows some of the results of this analysis. We see that even with a modest integrated luminosity of 10 fb^{-1} at $\sqrt{s} = 500$ GeV, the sensitivity to the form factors is quite good, at the level of 5–10% relative to SM couplings. In terms of real units, the 90% CL limits for F_{2A}^Z of ± 0.15, for example, correspond to a t-Z electric dipole moment of $\sim 8 \times 10^{-20}$ e-m. This type of analysis, which makes use of the full event information, should be a very general and powerful probe of the couplings. However, it is important to include the effects of background in such analyses. As shown in Ref. 18, this is unlikely to cause huge effects, and a larger data set can largely compensate. In fact, the assumed sample of 10 fb^{-1} is quite modest, especially given that no special beam energy is required, and one would expect the quoted errors to scale approximately with statistical error until the limits are very much smaller.

Table 4. A sample of the preliminary results from the global analysis described in the text. The upper and lower limits of the couplings in their departures from the SM values are given at 68% and 90% CL for 10 fb^{-1} and $m_t = 180$ $\mathrm{GeV/c^2}$. All couplings, with real and imaginary parts, can be determined in this way. The right-handed charged-current coupling is shown both for unpolarized and 80% left-polarized electron beam, whereas the other results assume 80% left-polarized beam only.

Form Factor	SM Value	Limits	
	(Lowest Order)	68% CL	90% CL
$F_{1R}^{W}(\mathcal{P}=0)$	0	± 0.13	± 0.18
$F_{1R}^{W}(\mathcal{P}=80\%)$	0	± 0.06	± 0.10
F_{1A}^{Z}	1	1 ± 0.08	1 ± 0.13
F_{1V}^{Z}	1	1 ± 0.10	1 ± 0.16
F_{2A}^{γ}	0	± 0.05	± 0.08
F_{2V}^{γ}	0	± 0.07	$^{+0.13}_{-0.11}$
F_{2A}^{Z}	0	± 0.09	± 0.15
F_{2V}^{Z}	0	± 0.07	± 0.10
$\Im(F_{2A}^{Z})$	0	± 0.06	± 0.09

5. Direct Top Yukawa Coupling Measurement

A fundamental tenet of the Standard Model is that the Higgs boson couples to fermions with a strength proportional to the fermion mass, as given by Eq. 4. This relationship clearly requires experimental scrutiny. As an example of alternative relationships, in many SUSY models Eq. 4 is modified by a factor $\cos\alpha/\sin\beta$, where α and β have their usual SUSY definitions. The large m_t implies that the top Yukawa coupling may be the only one which is accessible to experimental test. The sensitivity of the top threshold shape to Higgs exchange was discussed in Section 3.1 as a means toward Yukawa coupling measurement. Here we briefly discuss the possibilities for directly measuring this coupling in open top production. Figure 16 indicates representative diagrams which contribute to the relevant processes. One assumes that the Higgs boson(s) would have already been discovered, for example at LEP II, LHC, or FLC.

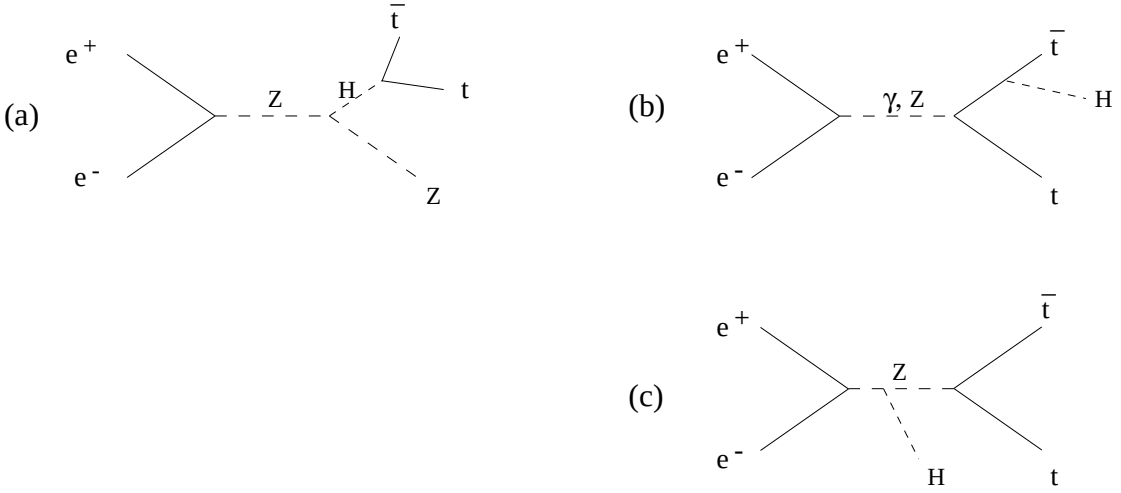


Fig. 16. Examples of processes discussed in the text for the study of the top-Higgs coupling.

Figure 16a represents production of Z^*H, where the Higgs is sufficiently massive to allow decay to $t\bar{t}$. This has been studied in Ref. 30, where it is found that for $m_t = 130$ GeV/c^2 and $M_H = 300$ GeV/c^2 it is possible to reconstruct ~ 30 events with $M(t\bar{t}) \approx M_H$ over a small background at the Higgs mass, and to measure the Yukawa coupling to 10% for 60 fb^{-1} and $\sqrt{s} = 600$ GeV. However, with realistic values of m_t, the cross section for this process drops rapidly, and would require extended running at high energy.

Rather than the heavy-Higgs, light-top scenario which is best for the process of Fig. 16a, we now find the more interesting possibility that of the so-called "Higgs-strahlung" represented by Fig. 16b, which is important for a light-Higgs, heavy-

top scenario. A study of this process was presented at this meeting[18] for $m_t = 180$ GeV/c^2, and is summarized here. Sensitivity to this process for a given M_H increases with $\sqrt{s}$. A cross section of about 1 fb is attained for $M_H = 100$ GeV/c^2 at $\sqrt{s} = 500$ GeV and for $M_H = 200$ GeV/c^2 at 1 TeV. A perfect reconstruction would produce a 10% or better measurement of the Yukawa coupling for $M_H < 240$ GeV/c^2, assuming an integrated luminosity of 50 fb^{-1}. While this seems promising, one must realize that these events, consisting typically of 6 or 8 jets, are not trivially reconstructed. And they must be separated from the background due to $t\bar{t}Z$ and $t\bar{t}$. A complete simulation was attempted for the $t\bar{t}H \to 8$ jets signal. It was found that due to its relatively high rate, the background from $t\bar{t}$ was most troublesome, and a signal to background ratio ~ 1 was determined from the simulations.

While this study is preliminary, it underscores the experimental challenge in studying this important process. Since we expect Higgs to decay primarily to $b\bar{b}$, then $t\bar{t}H$ events will consist of the final states 4 b-jet + 2-ℓ + 2-ν ($\sim$ 11%); 4 b-jet + qq' + $\ell\nu$ (44%); and 4 b-jet + 2-qq' (45%). Clearly, efficient b-tagging is an important tool for studying these events. And the subtleties associated with forming correct multi-jet masses in this busy environment will be important to study.

It turns out that the Higgs-strahlung process is also sensitive to deviations from the Standard Model involving extended Higgs sectors. The process represented by Fig. 16c also gives rise to the $t\bar{t}H$ final state. Interference between this and the processes represented by Fig. 16b is sensitive to extended Higgs sectors. In fact, Ref. 31shows that in many two-Higgs doublet models, including those favored by SUSY, this interference gives rise to large CP violation. They introduce CP-odd observables, which given roughly 100 fb^{-1} of data at $\sqrt{s} = 800$ GeV, could produce an observable CP asymmetry in $t\bar{t}H$ events, although the result depends on which parameters are chosen in the two-Higgs doublet model.

6. Summary

The discovery of top, especially the large measured mass, has brought the most important new input to the study of top physics at a high-energy linear e^+e^- collider. The main issues representing this physics has been covered, although to largely varying levels of detail and subtlety, in previous conference proceedings and journal articles. However, the large m_t has produced a qualitative change in the outlook for top physics. For example, the top threshold shape becomes less distinctive, with the corresponding measurement of parameters less precise. But the overwhelming change brought upon by the large mass is the sense that the top quark is truly special, and in fact may well play a major role in electroweak symmetry breaking, either directly or indirectly, or other physics at large mass. Hence, the measurement of the large top Yukawa coupling and the various electroweak couplings have taken on a new importance.

At this meeting, there were presentations which updated threshold studies for the measured m_t. These measurements will offer beautiful and unique tests of QCD, as well as unsurpassed measurements of top mass and width. A design year at a FLC at threshold would provide sensitivity to m_t and α_s at the level of 120 MeV/c^2 and 0.0025, respectively. Similarly, the sensitivity to the total top decay width is roughly 10%. Accelerator and detector designs have become sufficiently stable to make possible calculations which incorporate the systematics associated with luminosity spectra and backgrounds. This would allow determination of the limiting systematic errors at threshold. For example, is the measurement of beam energy, at the level of 100 MeV, really the limiting systematic for m_t measurement? With the large top mass, the contribution of Higgs exchange at threshold should become measureable, assuming that the systematics are under control.

Several presentations were given for direct Yukawa and electroweak coupling measurements. The Yukawa coupling measurement via the Higgs-strahlung process looks promising in principle, but in practice may present a significant challenge to the experimentalist, which will be very interesting to pursue. A complete set of measurements of electroweak gauge and dipole couplings of top to the charged and neutral currents is possible at a FLC. A modest sample of 10 fb^{-1} at $\sqrt{s} = 500$ GeV typically constrains these couplings, both real and imaginary parts, to within about 5–10% of their lowest-order Standard Model values.

Besides including increasing levels of reality to these studies based upon better simulations of signals and backgrounds, a few experimental techniques should prove generally applicable to these studies, but until now have not been fully utilized. The existence of electron beams with 80% polarization already exist at SLC, and this

level of polarization, or better, should be easily achieved at a FLC. For some measurements, for example of top couplings, the improvements with polarized beam are integral. But for other analyses, at the very least, polarization gives an increased top cross section (left-handed electrons) and dramatic reduction of W^+W^- background (right-handed electrons). The other demonstrated technique is precision vertex detection, where the small beam size and small, stable interaction point within FLC detectors represents a powerful asset which hopefully will be exploited in top physics studies at future meetings.

7. Acknowledgements

I sincerely thank the local organizers of LCWS95 for a truly splendid job of organization and for providing an enjoyable and stimulating environment. I also thank the editors for their patience. I have benifited greatly from helpful discussions with many colleagues, including K. Fujii, M. Peskin, J. Jaros, M. Fero, C. Schmidt, D. Burke, and T. Barklow.

8. References

1. F. Abe,*et al.* (CDF Collaboration), *Phys. Rev. Lett.* **74** (1995) 2626; S. Abachi,*et al.* (D0 Collaboration), *Phys. Rev. Lett.* **74** (1995) 2632.
2. K. Fujii, in *Conference on Physics and Experiments with Linear Colliders*, Saariselka, Finland, 1991.
3. P. Igo-Kemenes, in *Conference on Physics and Experiments with Linear Colliders*, Waikoloa, Hawaii, USA, 1993.
4. See K. Abe, *et al., Phys. Rev. Lett.* **73** (1994) 25, and references therein.
5. T. Barklow, contribution to these proceedings.
6. H.J. Schreiber, contribution to these proceedings.
7. M. Jezabek, J.H. Kuhn, and T. Teubner, *Z. Phys.* **C56** (1992) 653.
8. G. Jikia, *Phys. Lett.* **257B** (1991) 196; V.A. Khoze, L.H. Orr, and W.J. Stirling, *Nucl. Phys.***B378** (1992) 413.
9. K. Fujii, T. Matsui, and Y. Sumino, *Phys. Rev.* **D50** (1994) 4341.
10. C.J.S. Damerell, contribution to these proceedings.
11. E.A. Kuraev and V.S. Fadin, *Sov. J. Nucl. Phys.* **41** (1985) 466.
12. Pisin Chen, *Phys. Rev.* **D46** (1992) 1186.
13. V. Fadin and V. Khoze, *JETP Lett.* **46** (1987) 525 and *Sov. J. Nucl. Phys.* **48** (1988) 309; M. Strassler and M. Peskin, *Phys. Rev.* **D43** (1991) 1500; M. Jezabek, J. Kuhn, and T. Teubner, *Z. Phys.* **C56** (1992) 653;

M. Jezabek and T. Teubner, *Z. Phys.* **C59**, (1993) 669;
Y. Sumino, K. Fujii, K.Hagiwara, H. Murayama, and C.-K. Ng, *Phys. Rev.* **D47** (1993) 56.
14. M. Strassler and M. Peskin, *Phys. Rev.* **D43** (1991) 1500.
15. V. Fadin and V. Khoze, *JETP Lett.***46** (1987) 525 and *Sov. J. Nucl. Phys.* **48** (1988) 309.
16. R. Harlander, M. Jezabek, and J.H. Kuhn, TTP-95-25, hep-ph/9506292, 1995.
17. F. Zimmermann and T.O. Raubenheimer, "Compensation of Longitudinal Nonlinearities in the NLC Bunch Compressor", SLAC-PUB-95-7020, presented at *Micro Bunch*, Upton, N.Y., Sept. 1995.
18. M. Martinez,it et al., (European Top Physics Group), contribution to these proceedings.
19. Y. Sumino, K. Fujii, K.Hagiwara, H. Murayama, and C.-K. Ng,*Phys. Rev.* **D47** (1993) 56;
M. Jezabek, J. Kuhn, and T. Teubner, *Z. Phys.* **C56** (1992) 653.
20. P. Igo-Kemenes, M. Martinez, R. Miquel, and S. Orteu, in *Conference on Physics and Experiments with Linear Colliders*, Waikoloa, Hawaii, USA, 1993.
21. H. Murayama and Y. Sumino, it Phys. Rev. **D47** (1993) 82.
22. J. Kent, *et al.,* SLAC-PUB-4922, LBL-26977, 1989.
23. N.M. Frary and D. Miller, DESY 92-123A, Vol. I, 1992, p. 379.
24. See P.N. Burrows, contribution to these proceedings.
25. W. Bernreuther and M. Suzuki, *Rev. Mod. Phys.* **63** (1991) 313.
26. F. Cuypers, contribution to these proceedings.
27. M.E. Peskin and C.R. Schmidt, in *Conference on Physics and Experiments with Linear Colliders*, Saariselka, Finland, 1991.
28. G.A. Ladinsky and C.-P. Yuan, *Phys. Rev.* **D49** (1994) 4415; see also references therein.
29. C.R. Schmidt, SCIPP-95/14 (1995), hep-ph/9504434.
30. K. Fujii, in contribution by P. Igo-Kemenes, in *Conference on Physics and Experiments with Linear Colliders*, Waikoloa, Hawaii, USA, 1993.
31. S. Bar-Shalom, *et al., Phys. Rev.* **D53** (1996) 1162.